Multispectral digital colposcopy for *in vivo* detection of cervical cancer

Juan Manuel Benavides, Sung Chang, Sun Young Park, and Rebecca Richards-Kortum
Department of Biomedical Engineering, University of Texas, Austin, Texas 78712
Tel: (512) 471-3619
jmbr@mail.utexas.edu, kortum@mail.utexas.edu

Nick Mackinnon and Calum MacAulay
Department of Cancer Imaging, British Columbia Cancer Center, Vancouver, BC V5Z 4E6, Canada
Tel: (604) 877 6000
nmackinn@bccancer.bc.ca

Andrea Milbourne and Anais Malpica
University of Texas M.D. Anderson Cancer Center, Houston, Texas 77030
Tel: (713) 745 2564
amilbour@mail.mdanderson.org

Michele Follen
Department of Gynecologic Oncology, University of Texas M.D. Anderson Cancer Center, Houston, Texas 77030 and the Department of Obstetrics, Gynecology and Reproductive Sciences
University of Texas Health Science Center-Houston, Houston, Texas 77030
Tel: (713) 745 2564
mfollen@mail.mdanderson.org

Abstract: We present a multispectral digital colposcope (MDC) to measure multispectral autofluorescence and reflectance images of the cervix by using an inexpensive color CCD camera. The diagnostic ability of the MDC was evaluated by application of MDC spectral response to fluorescence and reflectance spectra measured from a large clinical trial. High diagnostic performance was achieved by use of only two excitation wavelengths: 330 and 440 nm. Good quality autofluorescence images of the human cervix were acquired *in vivo* with the MDC. Automated diagnostic algorithms correctly identified CIN (cervical intraepithelial neoplasia) lesions from MDC fluorescence images. The MDC has the potential to provide a cost-effective alternative to standard colposcopy and better direction of biopsies.

OCIS codes: (170.6510) Spectroscopy, tissue diagnostics; (110.2970) Image detection systems; (170.3890) Medical optics instrumentation

References and links

1. Cancer Facts and Figures, American Society of Cancer, 2001.
2. International Agency for Research in Cancer, 2002.
3. L. G. Koss, "The Papanicoloau test for cervical cancer detection: a triumph and a tragedy," J. Am. Med. Assoc. **261**, 737-743 (1989).
4. M. F. Mitchell, D. Schottenfeld, G. Tortolero-Luna, S. B. Cantor, R. and Richards-Kortum, "Colposcopy for the diagnosis of squamous intraepithelial lesions: a meta-analysis," Obstet. Gynecol. **91**, 626-631 (1998).
5. M. F. Mitchell, "Preinvasive diseases of the female low genital track," in *Operative Gynecology* D. M. Greshenson, A. DeCherney, and S. Curry, eds. (Saunders, Philadelphia, 1993), p. 231.
6. R. J. Kurman, D. E. Herison, A. L. Herbst, K. L. Noller, and M. H. Schiffman, "Interim guidelines for management of abnormal cervical cytology," J. Am. Med. Assoc. **271**, 1866-1869 (1994).
7. S. B. Cantor, M. Follen-Mitchell, G. Tortolero-Luna, C. Bratka, D. Bodurka, and R. Richards-Kortum, "Cost-effectiveness analysis of diagnosis and management of cervical squamous intraepithelial lesions," Obstet. Gynecol. **91**, 270-277 (1998).

#2291 - $15.00 US
Received March 28, 2003; Revised May 11, 2003

8. N. Ramanujam, M. F. Mitchell, A. Mahadevan, S. Thomsen, A. Malpica, T. C. Wright, N. Atkinson, and R. R. Richards-Kortum, "*In vivo* diagnosis of cervical intraepithelial neoplasia using 337-nm-excited laser-induced fluorescence," Proc. Natl. Acad. Sci. USA **91,** 10193-10197 (1994).
9. N. Ramanujam, M. F. Mitchell, A. Mahadevan, S. Thomsen, A. Malpica, T. C. Wright, N. Atkinson, and R. R. Richards-Kortum, "Spectroscopic diagnosis of cervical intraepithelial neoplasia (CIN) *in vivo* using laser induced fluorescence spectra at multiple excitation wavelengths," Lasers Surg. Med. **19**, 63-74 (1996).
10. N. Ramanujam, M. F. Mitchell, A. Mahadevan-Jansen, S. Thomsen, G. Staerkel, A. Malpica, T. Wright, N. Atkinson, and R. Richards-Kortum, "Cervical pre-cancer detection using a multivariate statistical algorithm based on laser induced fluorescence spectra at multiple excitation wavelengths," Photochem. Photobiol. **6**, 720-735 (1996).
11. A. K. Dattamajumdar, D. Wells, J. Parnell, J. T. Lewis, D. Ganguly, and T. C. Jr. Wright, "Preliminary experimental results from multi-center clinical trials for detection of cervical precancerous lesions using the Cerviscan system: a novel full-field evoked tissue fluorescence based imaging instruments," in 23rd Annual Meeting of IEEE-Engineering in Medicine and Biology, Istanbul, Turkey, October 2001.
12. I. Georgakoudi, B. C. Jacobson, M. G. Muller, E. E. Sheets, D. Badizadegan, D. L. Carr-Locke, C. P. Crum, C. W. Boone, R. R. Dasari, J. Van Dam, and M. S. Feld, "NADH and collagen as in vivo quantitative fluorescent biomarkers of epithelial precancerous changes," Cancer Res. **62**, 682-687 (2002).
13. R. Drezek, K. Sokolov, U. Utzinger, I. Boiko, A. Malpica, M. Follen, and R. Richards-Kortum, "Understanding the contributions of NADH and collagen to cervical tissue fluorescence spectra: Modeling, measurements, and implications," J. Biomed. Opt. **6**, 385-396 (2001).
14. I. Pavlova, K. Sokolov, A. Drezek, A. Malpica, M. Follen, and R. Richards-Kortum, "Microanatomical and biochemical origins of normal and precancerous cervical autofluorescence using laser scanning fluorescence confocal microscopy," submitted to Photochem. Photobiol. (2002).
15. N. Ramanujam, "Fluorescence spectroscopy of neoplastic and non-neoplastic tissues," Neoplasia **2**(1), 89-117, (2000).
16. I. Georgakoudi, B. C. Jacobson, J. Van Dam, V. Backman, M. B. Wallace, M.G. Muller, Q. Zhang, K. Badizadegan, D. Sun, G. Thomas, L. T. Perelman, and M. S. Feld, "Fluorescence, reflectance, and light-scattering spectroscopy for evaluating dysplasia in patients with Barrett's esophagus," Gastroenterology **120**, 1620-1629 (2001).
17. R. J. Nordstrom, L. Burke, J. M. Niloff, and J. F. Myrtle, "Identification of cervical intraepithelial neoplasia (CIN) using UV-excited fluorescence and diffuse-reflectance tissue spectroscopy," Lasers Surg. Med. **29**, 118-127 (2001).
18. A. Zuluaga, U. Utzinger, A. Durkin, H. Fuchs, A. Gillenwater, R. Jacob, B. Kemp, J. Fan, and R. Richards-Kortum, "Fluorescence excitation emission matrices of human tissue: a system for in vivo measurement and data analysis," Appl. Spectrosc. **53,** 302-311 (1998).
19. R. A. Zangaro, L. Silveira, R. Manoharan, G. Zonios, I. Itzkan, R. R. Dasari, J. Van Dam, and M. S. Feld, "Rapid multiexcitation fluorescence spectroscopy system for *in vivo* tissue diagnosis," Appl. Opt. **35**, 5211-5219 (1996).
20. A. Mayevsky, B. Chance, "Intracellular oxidation-reduction state measured in situ by a multichannel fiber-optic surface fluorometer," Science **217**, 537-40 (1982).
21. L. Burke, M. Modell, J. Niloff, M. Kobelin, G. Abu-Jawdeh, and A. Zelenchuk, "Identification of squamous intraepithelial lesions: fluorescence of cervical tissue during colposcopy," J. Lower Genital Tract Disease **3**, 159-162 (1999).
22. G. A. Wagnieres, W. M. Star, and B. C. Wilson, "In vivo fluorescence spectroscopy and imaging for oncological applications," Photochem. Photobiol. **68**, 603-32 (1998).
23. D. G. Ferris, R. A. Lawhead, E. D. Dickman, N. Holtzapple, J. A. Miller, S. Grogan, S. Bambot, A. Agrawal, and M. L. Faupel, "Multimodal hyperspectral imaging for the noninvasive diagnosis of cervical neoplasia," J. of Lower Genital Tract Disease. **5**(2), 65-72 (2001).
24. R. J. Nordstrom, L. Burke, J. M. Niloff, and J. F. Myrtle, "Identification of cervical intraepithelial neoplasia (CIN) using UV-excited fluorescence and diffuse-reflectance tissue spectroscopy," Lasers Surg. Med. **29**, 118-127 (2001).
25. A. Bogaards, M.C.G. Aalders, C.C. Zeyl, S. de Blok, C. Dannecker, P. Hillemanns, H. Stepp, and H. J. C. M. Sterenborg, "Localization and staging of cervical intraepithelial neoplasia using double ratio fluorescence imaging," J. Biomed. Opt. **7(2),** 215-220 (2002).
26. T. Wu, J. Y. Qu, T. H. Cheung, K. W. K. Lo, and and M. Y. Yu, "Preliminary study of detecting neoplastic growths *in vivo* with real time calibrated autofluorescence imaging," Opt. Express **11**, 291-298 (2003), http://www.opticsexpress.org/abstract.cfm?URI=OPEX-11-4-291
27. V. Trujillo, D. Sandison, U. Utzinger, N. Ramanujam, M. Follen Mitchell, and R. Richards-Kortum, "Method to determine tissue fluorescence efficiency in vivo and predict signal to noise ratio for spectrometers," Appl. Spectrosc. **52**, 943-951 (1998).
28. U. Utzinger, V. Trujillo, N. Atkinson, M. F. Mitchell, S. Cantor, and R. Richards-Kortum, "Performance estimation of diagnostic tests for cervical precancer based on fluorescence spectroscopy: effects on tissue type, sample size population, and signal to noise ratio," IEEE Trans. Biomed. Eng. **49**, 1293-1303 (1999).
29. S. K. Chang, M. Follen, A. Malpica, U. Utzinger, S. Gtaerkel, D. Cox, N. Atkinson, C. MacAulay, and R. Richards-Kortum, "Optimal excitation wavelengths for discrimination of cervical neoplasia," IEEE Trans. Biomed. Eng. **49**, 1102-1111 (2002).

#2291 - $15.00 US Received March 28, 2003; Revised May 11, 2003

30. N. Ramanujam, M. Follen Mitchell, A. Mahadevan, S. Thomsen, A. Malpica, T. Wright, N. Atkinson, and R. Richards-Kortum, "Development of a multivariate statistical algorithm to analyze human cervical tissue fluorescence spectra acquired *in vivo*," Lasers Surg. Med. **19**, 46-62 (1996).
31. R. J. Kurman and D. Solomon, *The Bethesda System for Reporting Cervical/Vaginal Cytologic Diagnosis* (Springer-Verlag, New York, 1994).

1. Introduction

Cervical cancer is the third most common type of cancer in women worldwide [1]. It is estimated that nearly 380,000 new cases are diagnosed each year, predominantly among the economically disadvantaged, in both developing and industrialized nations [2]. When detected early, cervical neoplasia is nearly 100% curable [3].

Cervical intraepithelial neoplasia (CIN) is usually detected by means of screening Pap smears from asymptomatic women. Patients with abnormal Pap smears are referred for colposcopy and possibly biopsy. During colposcopy, acetic acid is applied to the cervix, and areas with abnormal epithelium turn white [4-6]. The colposcope (low powered microscope used to examine the cervix with white light) is used to direct biopsies of the abnormal white areas. A pathologist then evaluates biopsies microscopically, and the diagnosis is based upon tissue morphology.

The Pap smear and colposcopy have reduced both the incidence and mortality of cervical cancer in countries where routine screening has been implemented [3]. Although the Pap smear is a relatively simple test, it has been reported to have false positive errors at the rate of 15-40% [4], leading to a large number of unnecessary colposcopies. The accuracy of colposcopy is highly dependent on the physician's expertise. In expert hands, colposcopy has been reported to have a high sensitivity (96%) and a low specificity (48%) when differentiating abnormal tissues (squamous intraepithelial lesions (SILs)) from normal tissues (normal squamous epithelia and inflammation)) [4]. Because of the low specificity, a biopsy is required to confirm disease. Biopsies dramatically increase the cost associated with colposcopy and delay treatment; over US$6 billion ($10^9$) are spent annually in the United States to evaluate and treat atypias [7]. In the developed world, there is a need for more objective, specific, and cost-effective screening and diagnostic techniques that could improve the accuracy of real-time detection, particularly in the hands of less-experienced practitioners. Nearly 80% of cervical cancers occur in the developing world, where resources for screening are not available. As a result many young women die of a preventable disease. In the developing world, there is a need for inexpensive screening and detection techniques that do not require expensive infrastructure, that are portable enough to be taken to small or remote population centers, and that do not require highly trained clinicians and pathologists.

Optical techniques have the potential to address these needs [7]. Optical measurements can be performed in a noninvasive manner to automatically identify CIN with high sensitivity and specificity, potentially reducing the frequency of unnecessary biopsies, and providing real time diagnosis with the possibility of immediate treatment by less experienced practitioners. In the developed world, the most important potential advantage of optical technologies is that they can combine screening, diagnosis and treatment into a single visit. This can reduce the enormous costs of diagnosis and loss to follow up. If the cost and complexity of optical technologies can be reduced sufficiently, they have the potential to dramatically increase the availability of screening and detection in the developing world.

Recent clinical studies have demonstrated the potential of both fluorescence and reflectance spectroscopies to detect cervical neoplasia [8-11]. Optical spectroscopy identifies cervical precancer by detecting both biochemical and architectural changes that accompany the development of dysplasia; recent studies show that fluorescence spectroscopy is sensitive to an increase in mitochondrial fluorphores in the precancerous epithelium and a decrease in stromal collagen cross linking [12-14]. Both reflectance and fluorescence spectroscopy can detect increased angiogenesis which accompanies precancer [15-17].

#2291 - $15.00 US Received March 28, 2003; Revised May 11, 2003

In vivo measurements of optical spectroscopy are most commonly conducted by using a fiber optic probe to deliver the excitation light and collect the remitted signal from the tissue [18-22]. Typically, the distal end of the probe is placed on the surface of the tissue and measurements are gathered at different sites. Although single point fluorescence and reflectance techniques have been used successfully to detect cervical neoplasia, such techniques are time consuming and are not practical to assess the large area of cervical tissue at risk during clinical practice.

Two-dimensional, multispectral imaging of cervical fluorescence and reflectance has the potential to greatly improve optical pre-cancer diagnosis. With two-dimensional imaging, the entire surface area of the cervix can be interrogated, potentially reducing the chance of sampling error and enabling evaluation of the colposcopically visible portion of the endocervical canal. Contextual classification techniques may increase diagnostic accuracy compared to single point measurements. Several groups have recently presented promising systems to evaluate optical images of cervical fluorescence and reflectance [23-26]; however, in many cases, the instrumentation is complex and expensive.

The goal of this study was to develop a cost-effective multispectral imaging system for the detection and diagnosis of cervical neoplasia and to predict its feasibility to detect CIN. We evaluated the potential of modifying a standard colposcope with video camera adapter to measure reflectance and fluorescence images using an inexpensive (<$500) color video camera (CV S3200, JAI, Japan) with a sensitivity of 0.09 lux. This camera has 8 by 8 μm pixels and can detect $8e^{-15}$ W per pixel. Here, spectral sensitivity is provided by the three color channels of the CCD

Trujillo *et al.* determined the fluorescence efficiency of normal and abnormal cervical tissue [27]. The fluorescence efficiency (FE), which is defined as the ratio of emitted fluorescence power to the incident illumination power, varies from 0.004 (for normal tissue at 337 nm excitation) to 0.0003 (for precancer at 460 nm excitation). Based on these FE values, we estimated that $1.3mW/cm^2$ illumination incident on the tissue will result in $2\ e^{-14}$ W per pixel at the CCD detector. Hence, we predicted that this camera would be able to measure fluorescence images from the cervix with SNR of 10 for a single frame.

Utzinger *et al.* previously examined diagnostic capability versus SNR with fluorescence emission spectra [28]. They found that diagnostic performance was largely unchanged as the SNR dropped from 300 to about 5. Only when SNR dropped below 5 did performance drop substantially. In addition, we have the advantage of signal processing provided by the eye when viewing images, thus our target SNR was 10.

To select the optimal excitation wavelengths for the MDC and to assess whether the three channels of emission wavelength sensitivity are sufficient for diagnosis, we first simulated the expected diagnostic performance of the MDC using excitation emission matrices from a large clinical trial. The design of the MDC was based on this simulation. Finally, we demonstrate that this inexpensive system can be used to obtain reflectance and fluorescence images of cervical tissue in less than 1 s. The algorithm developed based on the spectral data was applied pointwise to the MDC images; results show good correlation with independent histopathologic analysis.

2. Materials and methods

2.1. Multispectral imaging colposcope prototype

A system diagram of the MDC system is depicted in Fig. 1. The system is composed of three subsystems: (1) a light source, which provides monochromatic and broadband illumination and a fiber optic probe that directs the excitation light to the tissue; (2) a colposcope with integrated video camera adaptor and a selection of longpass filters; and (3) a video rate color CCD camera with A/D frame grabber used to spectrally resolve the fluorescence and reflectance images from the tissue. The operation of the CCD camera was controlled using a PC computer and a LabVIEW program (National Instruments, Austin, TX). Below, each subsystem is described in detail.

#2291 - $15.00 US Received March 28, 2003; Revised May 11, 2003

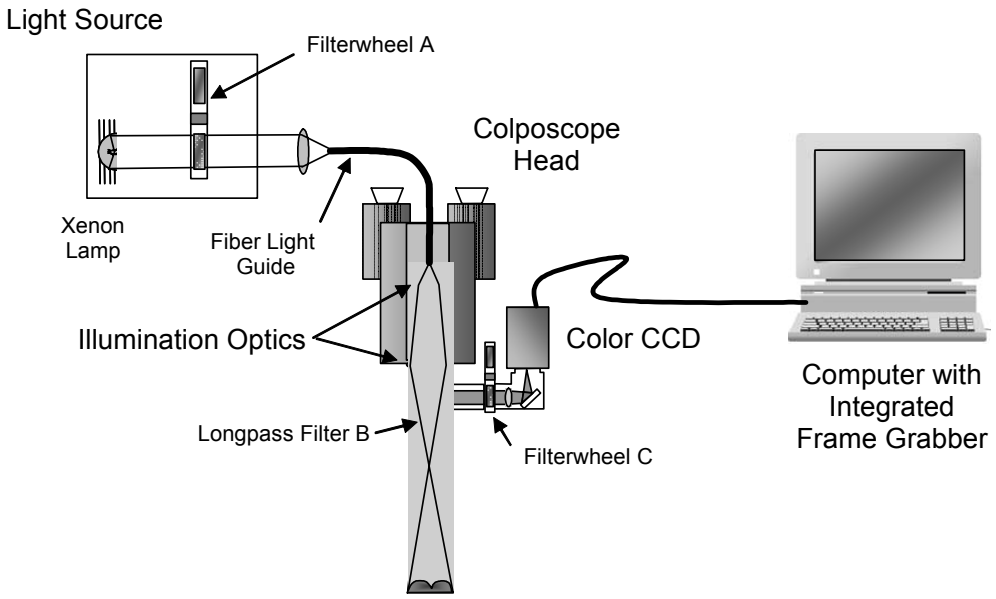

Fig. 1. System diagram of the MDC.

The light source is based on a Xenon arc lamp with an integrated parabolic reflector. The parabolic reflector collects the light from the light bulb and produces a collimated output beam. The fluorescence excitation light is produced using bandpass filters enclosed in a motorized filterwheel (filterwheel A) located in the collimated region of the beam. Filterwheel A also contains a filter that blocks UV light and near infrared light when the device is used in reflectance mode. A 25 mm focal length UV lens focuses the light onto a 0.25 inch core diameter quartz fiber light guide. A combination of lenses is attached to the distal end of the probe (illumination optics). This lens combination produces a 3.5 cm diameter illumination spot at a working distance of 30 cm. The measured illumination intensity at this working distance was approximately 0.25 mW/cm^2 at 345 nm excitation and 2.4 mW/cm^2 at 440 nm excitation.

The MDC was built around a commercially available tilt-stand colposcope (Model 1DL, Leisegang, Germany). This colposcope produces stereoscopic vision at 7.5X magnification. The original halogen lamp of the colposcope was removed to accommodate the fiber optic light guide. Figure 2 shows a photograph of the MDC system.

#2291 - $15.00 US Received March 28, 2003; Revised May 11, 2003

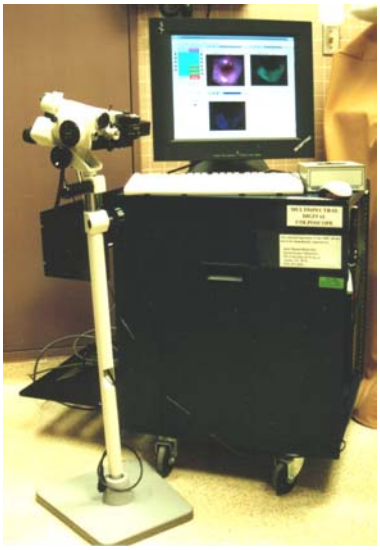

Fig. 2. Picture of the MDC system.

A commercially available camera adaptor designed for the Leisegang colposcope was chosen to mount the camera. We modified the camera adaptor to incorporate two longpass filters. The longpass filter with the lowest cutoff wavelength (longpass filter B) was attached in front of the objective lens in order to prevent UV light from reaching the collection optics at all times, thus preventing the optics from autofluorescing. We incorporated a manual filterwheel containing the longpass filter with the highest cutoff wavelength (longpass filter C). In this way, broadband illumination images could be acquired and fluorescence images could be acquired at different two different cutoff wavelengths.

The camera is an analog video rate color CMY camera (CV S3200, JAI, Japan). The dynamic range of each channel is 8 bits. The camera CCD is sensitive to CMY colors; however, the camera transforms the measured CMY values into RGB values. Figure 3 shows the spectral response curves for the JAI camera. The camera has a sensitivity of 0.09 lux at 50% video rate and maximum gain level. The camera was connected to a Pentium IV computer via a National Instruments frame grabber (PCI 1411, National Instruments, Austin, TX). An S-video cable was used to connect the camera to the frame grabber. A LabVIEW based program was developed to acquire, save, process, and display the images.

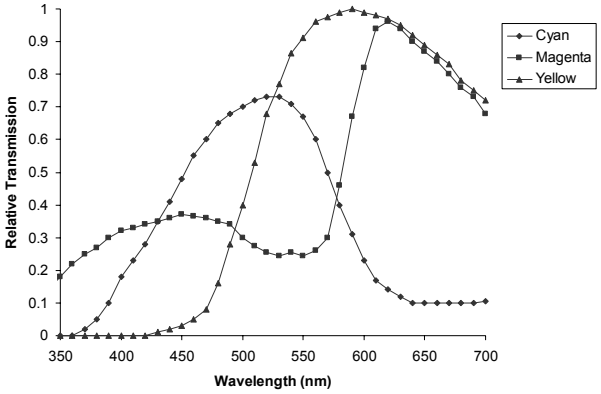

Fig. 3. Spectral response curves of the CV S3200 JAI color camera.

#2291 - $15.00 US Received March 28, 2003; Revised May 11, 2003

2.2. Diagnostic performance simulation

In order to determine if the three channel spectral response of the MDC would provide valuable diagnostic information, their diagnostic performance for the diagnosis of pre-cancer was estimated. The evaluation was performed on two excitation wavelength regions identified in earlier work as optimal for detection of high grade SIL, 330 to 360 nm and 440 to 470 nm at 10 and 20 nm bandwidths [29].

The estimation was performed using spectral data from a 146 patient clinical trial where fluorescence excitation emission matrices and reflectance spectra were measured from 351 pre-cancerous and normal cervical sites. The instrumentation used during the clinical trial has been previously described in detail [18, 29]. This system uses a fiber optic probe to interrogate a small area of tissue (~2mm) and can measure fluorescence emission spectra at 16 excitation wavelengths ranging from 330 to 480 nm at 10 nm intervals, and resolve emission spectra with 5 nm spectral resolution.

The spectral response of the MDC was simulated by multiplying the measured fluorescence spectra by the JAI color camera CMY spectral response curves and integrating the area under the curve. For each emission spectrum we obtained three values (C, M, and Y). Each value corresponded to the spectral overlap between the color channel and the emission spectrum. For each measured site, we simulated the spectral response of the MDC from two different emission spectra, thus we obtained two sets of CMY values. Then, we used these simulated CMY values as input to a classification algorithm to discriminate data from two diagnostic categories. We considered pairwise discrimination of all combinations of diagnostic categories. The performance of the classification algorithm (sensitivity and specificity) was evaluated relative to histopathologic diagnosis using cross-validation. Finally, we compared the performance obtained using the simulated MDC data to that obtained using the full spectral data.

The method of algorithm development has been described in detail previously [29]. When evaluating the performance of the classification algorithm applied to the full spectral data, the data set underwent dimensionality reduction using principal component analysis (PCA), as described in [29]. Eigenvectors accounting for 75% of the total variance were used as input to this classification algorithm.

To select the most promising excitation wavelengths for discrimination of the different diagnostic classes in the MDC, wavelengths that yielded the highest diagnostic performance for the full spectrum analysis were explored. Emission spectra with 10 nm and 20 nm bandwidth excitation wavelengths were used. Data were originally measured with 10 nm excitation bandwidth; emission spectra with 20 nm excitation bandwidth were simulated by adding two adjacent emission spectra measured at 10 nm bandwidth excitation.

2.3. System fluorescence imaging performance

The MDC fluorescence imaging performance was tested by imaging different standard samples including solutions of two fluorescent compounds, Exalite (1.33 mM in ethylene glycol) and flavin adenine dinucleotide (FAD) (0.016 mM in PBS) solution. Both, the Exalite and the FAD solution were contained in 40 x 40 mm quartz cuvettes to cover the MDC's entire field of view.

The MDC was used to measure white light and fluorescence images of the intact cervix during colposcopy. The study protocol was reviewed and approved by the Institutional Review Boards at The University of Texas M.D. Anderson Cancer Center and The University of Texas at Austin. Eligible patients included those over the age of 18 who were not pregnant, who were referred for treatment of cervical SIL at the Colposcopy Clinic at the UT M.D. Anderson Cancer Center. After signing informed consent, all patients underwent a complete history and physical exam and pan-colposcopy of the vulva, vagina and cervix. During colposcopy, the MDC was used to image the cervix with white light illumination, and to image autofluorescence at two excitation wavelengths. Images were acquired prior to and

#2291 - $15.00 US Received March 28, 2003; Revised May 11, 2003

approximately two minutes after application of 6% acetic acid. For each illumination condition video was obtained for 5-10 s at a frame rate of 2 frames/s. Images presented here are single frames.

Following colposcopy and fluorescence measurement, the ectocervix was removed during a loop electrosurgical excision procedure (LEEP). The LEEP specimen removed a portion of the cervix which was approximately 2.5 cm in diameter and 1 cm in depth. Immediately after removal, the ecotcervical margin was stained with blue ink and the deep margin was stained with black ink. A stitch was placed at the 12 o'clock position of the specimen. The sample was fixed in formalin and sectioned radially into 12 specimens. Transverse sections were obtained at each clock position, stained with hematoxylin and eosin and examined by the study histopathologist (AM). Standard diagnostic criteria were used [31] and diagnostic categories included: normal squamous epithelium, normal columnar epithelium, human papilloma virus (HPV) infection, grade 1 cervical intra-epithelial neoplasia (CIN 1), grade 2 cervical intra-epithelial neoplasia (CIN 2), and grade 3 cervical intra-epithelial neoplasia (CIN 3).

2.4 Image processing and classification of tissue

In order to identify the abnormal areas in the MDC fluorescence images, each pixel of a cervical image was classified to be either SN or HG according to a classification algorithm. The values used by the classification algorithm were obtained from both the 345 nm and the 440 nm excitation fluorescence images. Three ratios were calculated by dividing each color channel by the sum of the three channels (i.e. R/(R+G+B), G/(R+G+B), B/(R+G+B)) from every pixel of a fluorescence image. As a result, each pixel of the cervical image was classified according its six corresponding ratios. The simulated MDC data set corresponding to 345 nm and 445 nm excitation used in the diagnostic performance algorithm was used as the training set for the classification algorithm. Although the training set was simulated by filtering the full spectral data by the color camera CMY curves, we used the RGB values outputted by the camera to calculate the ratios for the classification algorithm.

3. Results

The data set used to simulate the performance of this MDC consisted of 233 normal squamous sites, 23 columnar sites, 63 LGSILs and 31 HGSILs. 107 of the 233 squamous normal sites included inflammation and/or metaplasia. 40 showed inflammation only, 14 showed metaplasia only, and 53 showed both inflammation and metaplasia. Figure 4 compares the specificity and sensitivity for separating SN versus CN, SN versus LGSIL, SN versus HGSIL, CN versus LGSIL, and CN versus HGSIL when using the full emission spectra and the simulated MDC spectral response at 330 and 440 nm excitation wavelengths. In general, the diagnostic performance simulated for the MDC is comparable to that obtained using the full spectral data for all pairs of diagnostic categories.

#2291 - $15.00 US Received March 28, 2003; Revised May 11, 2003

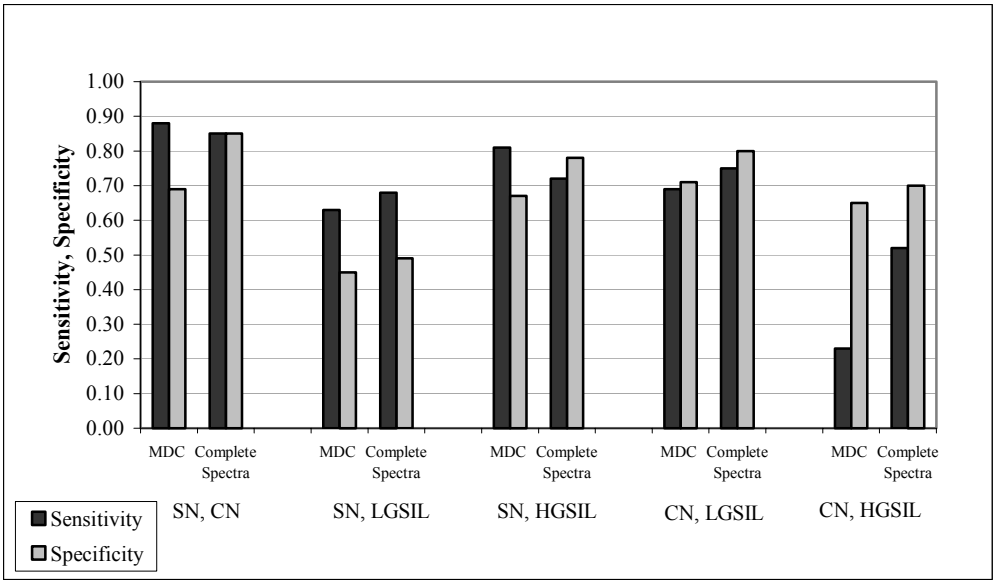

Fig. 4. Se, Sp values for the classification algorithm when applied to simulated MDC data and the complete spectra at 330 nm and 440 nm excitation wavelengths.

In both cases, the algorithm performs well for separating SN versus CN, SN versus HGSIL, and CN versus LGSIL. The performance is lower when separating SN versus LGSIL and CN versus HGSIL.

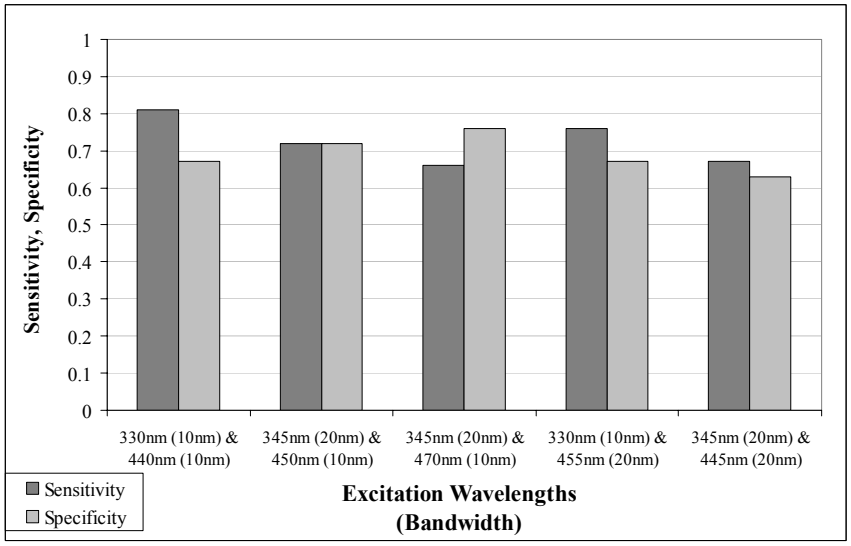

Fig. 5. Se and Sp of the four best performing excitation wavelengths and bandwidths combinations for the discrimination between SN and HGSIL. The fifth combination shows Se and Sp for the selected excitation wavelengths for the MDC.

Figure 5 compares the sensitivity and specificity of the four best performing excitation wavelength and bandwidth combinations for discrimination between SN and HGSIL. The excitation wavelengths are listed in descending order of the sum of the cross-validated sensitivity and specificity. Performance was best with the combination of 335-340 nm and

#2291 - $15.00 US
Received March 28, 2003; Revised May 11, 2003

440-445 nm excitation with 10 nm bandwidth. However, we found the autofluorescence of the optical system to be too high at 335 nm excitation wavelength. Excitation at 345 nm gave similar simulated diagnostic performance, while minimizing device autofluorescence. In general, increasing the excitation bandwidth from 10 nm to 20 nm did not significantly change the simulated diagnostic performance. The additional excitation power available with 20 nm bandwidth increased image SNR. Based on these results, we selected exciation wavelengths of 345 nm and 440 nm with 20 nm bandwidth. The expected performance of the MDC under these conditions is also shown in Fig. 5.

Table 1. Selected bandpass and longpass filters for the two different imaging fluorescence modes.

Fluorescence Mode	Bandpass Filters Center λ (Δλ)	Longpass Filters Cutoff λ
1	345 nm (20 nm)	388 nm
2	440 nm (20 nm)	468 nm

Figure 6 shows the fluorescence image of the Exalite solution at 345 nm excitation and its corresponding red, green and blue images.

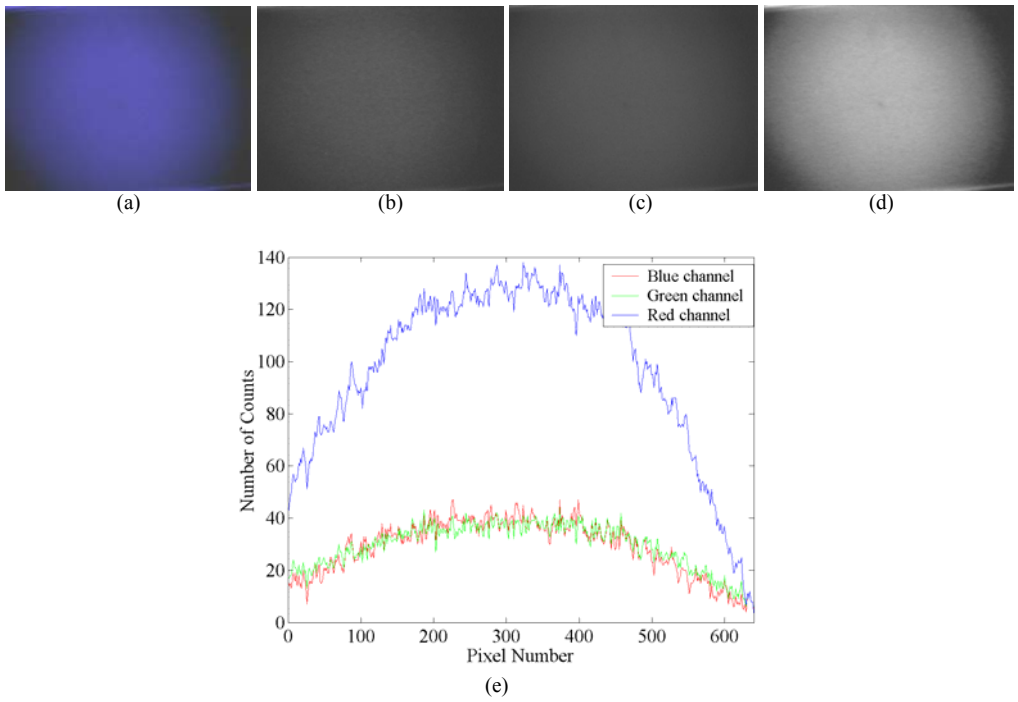

Fig. 6. (a) Fluorescence image of Exalite at 345 excitation, (b) red, (c) green, and (d) blue channels. (e) Intensity versus pixel number from the central horizontal cross section of images in (a) – (c) illustrating nonuniform illumination at edges of the field.

The red, blue, and green images are presented using the same grayscale. The peak emission wavelength of Exalite is expected to be 380 nm, which lies in the blue region of the spectrum. The mean intensity of the blue image is four times larger than the mean intensities of the green and red images.

#2291 - $15.00 US
Received March 28, 2003; Revised May 11, 2003

Figure 7 shows the fluorescence image of the FAD solution at 440 nm excitation and its corresponding red, green and blue images. The peak emission wavelength of the FAD is expected to be 530 nm, which lies in the green spectral region. In this case, the mean intensity of the green image is almost five times larger and two times larger than the mean intensity of the blue and red images, respectively. This result also agrees well with the expected peak emission wavelength of FAD. These images demonstrate that the system can detect fluorescence signals which are similar in intensity to cervical tissue.

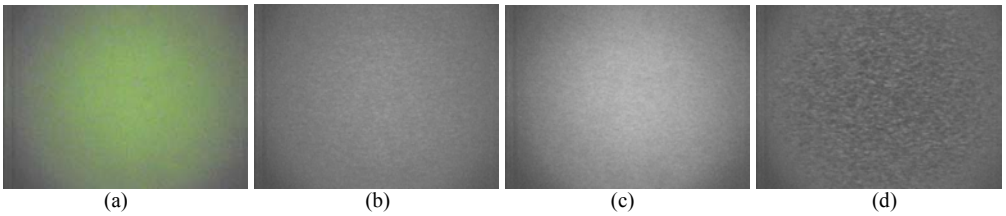

Fig. 7. (a) Fluorescence image of FAD at 440 excitation, (b) red, (c) green, and (d) blue channels.

The MDC field of view (FOV) was determined to be 30 mm by 22.5 mm. However, Figures 6 and 7 reveal that the light source does not provide a uniform illumination across the entire FOV. Both the Exalite and the FAD images show that the illumination field is circular in shape and its intensity decreases radially from the center of the image. Figure 6 (e) shows a central horizontal crossectional plot extracted from the Exalite image. This plot shows a relatively uniform intensity across a circular region of about 300 pixels in diameter centered at the middle of the illumination field. Outside this region, the intensity drops as described by the plot. Areas of 50 by 50 pixels at the corners of the images reach mean intensities as low as 16 counts.

Figure 8 shows an image corresponding to a background measurement. The image was acquired with both the room lights and the MDC light source turned off. The background level was calculated to be 17 counts for the green channel and 15 for both the green and the blue. The noise level is approximately equal to 5 counts for all the channels.

Fig. 8. Background image measured with the room lights and the MDC light source off.

To assess the level of device fluorescence we imaged a standard with no autofluorescence, but with diffuse reflectance properties similar to the cervix. We have found a frosted quartz cuvette to be ideal for this purpose, with no autofluorescence and about 15% diffuse reflectance. Figures 9(a) and 9(b) show images of a frosted cuvette illuminated with 345 nm and 440 nm excitation light respectively. The mean intensities calculated from the 345 nm excitation image were 26, 27, and 35 counts for the red, green and blue channels respectively. The mean intensities calculated from the 440 nm excitation image were 24, 28, and 24 counts for the red, green, and blue channels, respectively. These images revealed that the autofluorescence levels of the MDC were not significant when compared to the Exalite and FAD images.

#2291 - $15.00 US Received March 28, 2003; Revised May 11, 2003

(a) (b)

Fig. 9. Frosted cuvette images at (a) 345 nm and (b) 440 nm excitation.

Figure 10 shows the reflectance and fluorescence images measured from a patient with both CIN I and CIN II lesions.

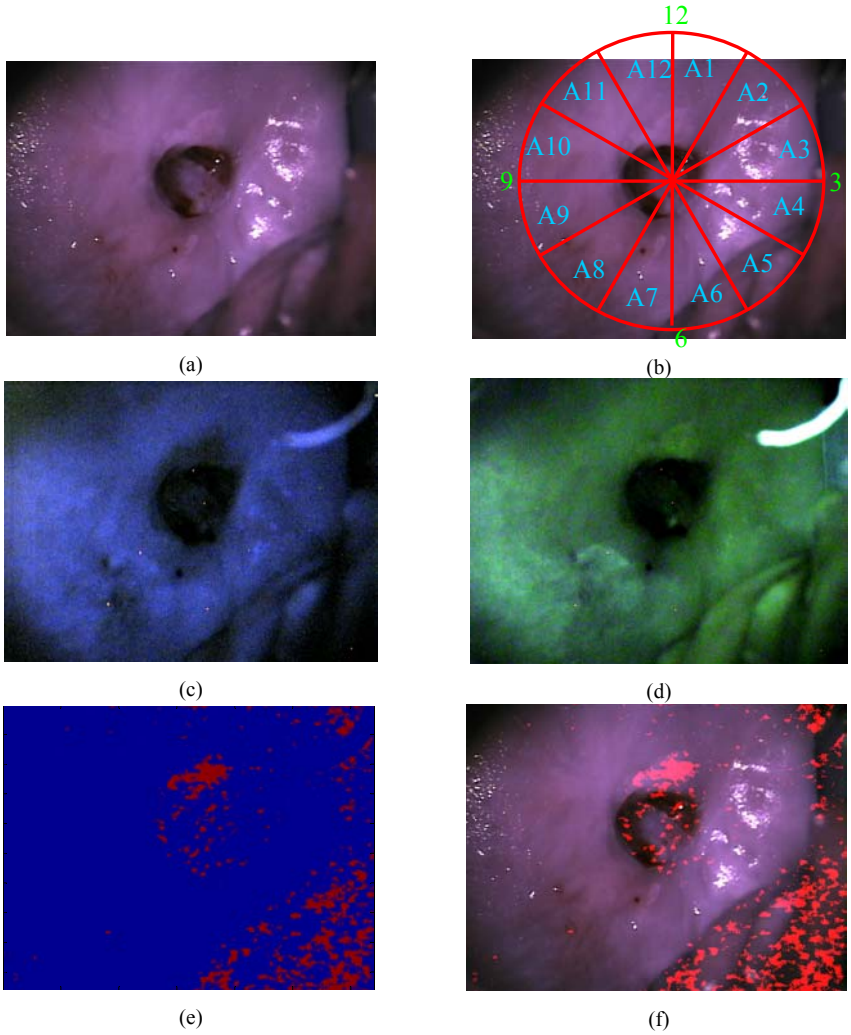

Fig. 10. Reflectance and fluorescence images of a patient with both CIN I and CIN II lesions. (a) shows the reflectance image and (b) shows the pathology section code used to map the pathology diagnosis to the fluorescence images. (c) and (d) show the fluorescence images taken at 345nm and 440 nm respectively. These images were taken after the application of acetic acid. (e) shows the results from the classification algorithm for SN versus HG. Blue areas indicate SN tissue and red areas indicate HG tissue. (f) shows the areas classified as HG overlaid over the reflectance image.

#2291 - $15.00 US Received March 28, 2003; Revised May 11, 2003

These images were measured after the application of acetic acid. Figure 10(a) shows the reflectance image and Fig. 10(b) shows the pathology section code used to correlate the pathology diagnosis to the fluorescence images.

The preliminary pathology results indicate a CIN III lesion surrounding the os in sections A1, A2, A10, A11, and A12. The pathology also reveals a CIN III lesion within the endocervix. Fluorescence images at 345 nm and 440 nm excitation can be seen in Figs. 10(c) and (d), respectively. Both images were acquired immediately after the reflectance image. We estimated a SNR equal to 23 for the 345 nm excitation image and a SNR equal to 28 for the 440 nm excitation image. The 345 nm excitation fluorescence image reveals a decrease in fluorescence intensity at the locations of both lesions. However; the 440 nm shows an increase in intensity over the CIN III lesion surrounding the os. The fluorescence intensity over the CIN III endocervical lesion is higher for the 440 nm image than for the 345 nm image. Both images reveal strong fluorescence of a hair strand at their upper right corner.

The results from the classification algorithm when classifying squamous normal (SN) versus high grade (HG) tissue can be seen in Fig. 10(e). The blue areas correspond to SN and the red areas to HG. Fig. 10(f) shows the HG results overlaid onto the reflectance image. Even though some outliers are present, there appears to be significant correlation between the classification algorithm results and the pathology results. Notice that the tissue identified as HG at the lower right corner of the image is really vaginal epithelium. It is also interesting to see that the hair fluorescence was not classified as an abnormality.

4. Discussion

In summary, we determined that the MDC can provide significant diagnostic information for the discrimination of SN versus HGSIL, SN versus CN, and CN versus LGSIL with only three channels of emission wavelength sensitivity. In a previous study, it was determined that it is possible to discriminate between pairs of histologic classifications when data from two excitation wavelengths are combined [30]. Moreover, it was determined that excitation wavelengths ranging from 330 to 360 nm and 440 to 470 nm appeared important when a diagnostic algorithm is used that separates SN and CN, SN and HGSIL, and CN and LGSIL. However, this analysis was based on emission spectra measured at 5 nm intervals and at excitation wavelengths of 10 nm in bandwidth. Figure 3 shows that diagnostic performance obtained when using only three spectral features measured at two different excitation wavelengths does not decrease significantly when compared with use of the entire emission spectra. However, these results also show that the performance is low when discriminating between SN and LGSIL, and CN and HGSIL.

The classification algorithm still performs well when it is applied to fluorescence emission spectra at excitation wavelengths of 20 nm in bandwidth as shown in Fig. 4. Based on these results and considering that wider excitation bandwidths yield to fluorescence images with higher SNR, we selected the bandpass filters shown in Table 1 for the MDC excitation illumination. Although the simulations showed UV excitation light around 330 nm to be promising for detection of precancers, we avoided using light below 340 nm to reduce system auto fluorescence and improve the excitation efficiency.

Figures 5 and 6 show the ability of the MDC to detect fluorescence from a common laser dye (Exalite) and a biological fluorophore (FAD). These images reveal that the illumination provided by the MDC is not uniform over the FOV. The illumination profile is circular and the intensity is uniform over a diameter approximately equal to 300 pixels. The illumination drops significantly along the edges of the image. However, by imaging these standards, we can preprocess the *in vivo* fluorescence images to account for intensity changes across the FOV.

The ability of the MDC to image tissue autofluorescence *in vivo* at two different excitation wavelengths is depicted in Fig. 10. Spectral information of the fluorescence images is provided by the color channels of the CCD camera. A sequence of fluorescence images measured in less that 1 s can be processed to provide a single fluorescence image with higher SNR. Patient movement during the acquisition of images can result in loss of spatial

#2291 - $15.00 US Received March 28, 2003; Revised May 11, 2003

resolution. However, the sequences of images can be digitally processed to reduce motion artifacts. The results from the classification algorithm illustrated in Figsx 10(e) and 10(f) demonstrate that the spectral information acquired with a color CCD camera can prove to be valuable when discriminating between normal and precancerous tissue.

5. Conclusion

We have built a multispectral digital colposcope based on a commercially available colposcope and an inexpensive video rate color camera. The system can use the color camera's CMY filters to extract three features from an emission spectrum. No fluorescence stain is needed, because the MDC targets tissue autofluorescence. Our simulations predict that fluorescence images measured and resolved with the MDC at two different excitation wavelengths can provide significant diagnosis information for discrimination of SN versus CN, SN versus HGSIL, and CN versus LGSIL. The measured fluorescence images yielded SNR values higher than 10 and proved to be useful for classifying SN tissue versus HG tissue. The performance estimations presented here indicate that performance is similar to current spectrometer-based systems. However, the availability of multipixel image data will enable the development of multivariate classifiers that utilize nearest-neighbor information to recognize and delineate the borders of CIN lesions, which are expected to further improve diagnostic performance. We believe that the MDC has the potential to provide a cost-effective *in vivo* tool to detect precancerous changes, and the system will be used in clinical trials on the cervix in the near future.

#2291 - $15.00 US Received March 28, 2003; Revised May 11, 2003